Hindawi
Journal of Sensors
Volume 2019, Article ID 6108297, 8 pages
https://doi.org/10.1155/2019/6108297

Research Article

Vibration Suppression and Isolation for Rapeseed Grain Cleaning Loss Sensor

Lizhang Xu, Zhenwei Liang, Chuncai Wei, Xiaoyu Chai, and Yaoming Li

Key Laboratory of Modern Agricultural Equipment and Technology, Ministry of Education, Jiangsu University, Zhenjiang Jiangsu 212013, China

Correspondence should be addressed to Zhenwei Liang; liangzhenwei518@126.com

Received 5 April 2019; Accepted 16 August 2019; Published 30 November 2019

Academic Editor: Tomasz Wandowski

Rapeseed cleaning loss is an important factor to weigh rapeseed combine harvester performance. With the development of sensor technology, establishing a rapeseed cleaning loss monitoring system can be interesting and necessary. However, the rapeseed combine harvester made in China is always with larger vibration, which is not beneficial for sensor monitoring accuracy. Experiment results indicate that inertia force from vibrating sieve unbalanced motion has the greatest influence on the monitoring accuracy of the sensor in its installation position. To reduce the effect of vibration on monitoring accuracy of the sensor, the vibration absorption and isolation structure for cleaning loss sensor has been designed. Moreover, the vibration isolation design was performed on the basis of vibration suppression. The vibration isolation rubber was designed to isolate the vibration at the joint of the sensor with the frame. The experimental results shown that the above design can reduce the vibration disturbance and highlight the grain collision signal greatly, which is beneficial for improving the sensor discrimination ability.

1. Introduction

Rapeseed is one of the important crops for edible oil, and China is the largest rape oilseed producer in the world with an annual production of 12 million tons, which accounts for approximately 35% of global rape oilseed production. However, compared to other major producing areas or countries in the world, the mechanization level of rape harvest in China is relatively low (under 16.88%), and the rapeseed is still harvested manually owing to poor cleaning performance of current rape combine harvesters (Xu, et al., 2008). At present, the rapeseed cleaning loss calculation is mainly done manually which has the main disadvantage of having a larger corresponding calculation error and always lagging behind, which cannot provide current grain loss level for the operator to adjust relevant working parameters in time and cause direct income loss.

Many research works had been carried out to develop sensors to monitor grain cleaning loss in combines, and cleaning loss sensors have become an indispensable accessory in combine harvesters made by some European and U.S. agricultural machinery companies [1–8]. There are also some scientists from China who carried out some research on grain loss monitoring by using PVDF, multicontact induction film, and piezoceramics as sensitive elements in recent years (Li 2006 & 2009; [9]; Liang et al., 2013; Liu et al., 2013). However, field experiment results indicated that it is not effective to monitor the rapeseed sieve loss using the sensor developed for rice and wheat owing to severe vibration in the installation place. Research also indicates that the oscillating sieves are influenced by the inertial force of rotary motion in addition to external loads during the cleaning process of a combine harvester [10]. Therefore, it is necessary to reduce the effect of oscillating sieve inertial force as much as possible.

On the basis of our previous study on rapeseed grain and MOG (material other than grain) impact behavior with the sensor [11] which lay a good foundation for impact signal processing design, in this paper, the vibration absorption and isolation structure has been designed to upgrade the sensor monitoring accuracy. Firstly, inertial force balance to the sieve has been carried out by adding balanced counterweight to sieve on the basis of a vibration test by DH5902

and ADAMS simulation analysis. Then, the vibration isolation structure to the sensor was designed on the basis of vibration suppression. The ideal stiffness of the rubber was obtained, and experimental results indicated that the disturbance signal amplitude was reduced significantly.

2. Vibration Signal Sampling and Analysis

2.1. Measurement Device and Method. The vibration test was carried out in the TH988 type tangential-longitudinal flow full feeding combine harvester (Wuxi Combine Harvester Co., Ltd., China). The threshing and cleaning device (Figure 1) working processes can be summarized as follows: the threshed outputs from the tangential threshing cylinder fall into the grain pan, on which they are conveyed towards sieve front. Subsequently, the threshed outputs from the longitudinal axial-flow threshing cylinder drop onto the sieve directly. The combined effects of airflow and sieve remove light materials from the threshed outputs to assist in positioning grains and moving particles along the sieve surface. Finally, the grains passing through sieve openings are gathered and conveyed to the grain tank by the grain auger. Some threshed outputs that do not pass through the sieve openings fall into the tailing auger which are conveyed to the sieve from the tailing window for the second cleaning.

The acceleration test system includes acceleration sensors, signal collectors, signal processing software, and a PC [12]. The type of the 3-directional acceleration sensor is PCB-356A16 with a range of 0-50 g and frequency response of 0.3-6000 Hz. The signal acquisition instrument is DH5902 dynamic signal acquisition instrument (Donghua, Co., Ltd., Jingjiang, China). The sampling bandwidth is 100 kHz. The signal processing software is DHDAS5902-net dynamic signal analysis software (Donghua, Co., Ltd., Jingjiang, China).

As the grain loss sensor was connected to the two sides of the rack at the tail of the vibrating sieve and there are mainly reciprocating motion of the vibrating sieve and rotating motion of the roller near its installation, the vibration from the two exciting sources and the sensor installed position are the main tested points, and the specific measurement point distributions are shown in Table 1. Considering the actual working state and harvesting conditions, the vibration test was carried out under the harvesting condition. The location of the acceleration sensors on the combine harvester is shown in Figure 2.

Firstly, a 3-directional acceleration sensor was arranged according to the measuring point position as shown in Table 1, respectively: open the wireless Wi-Fi transmitter to realize the communication between the signal acquisition instrument and the computer, then set a series of parameters in the signal acquisition software DHDAS5902-net, and start the combine harvester. The combine harvester forward speed was stable at 1.0 m/s. Three tests were carried out, and the collected data were stored on the computer after the tests were completed.

2.2. Spectrum Diagram Analysis for Signal from Different Sensors. Fast Fourier Transform (FFT) was used to obtain the signal spectrum from the time-domain data measured at the abovementioned 3 measuring points. As vibration in the Z direction and X direction has a great influence on the sensor's monitoring accuracy, therefore, only vibration in the X direction and Z direction was analyzed.

Under the simulated harvesting condition, the frequency spectrum analysis showed that the main vibration frequency of the threshing rotor is 14.65 Hz, its vibration in the X and Z directions is not significant, and it has a little effect on monitoring accuracy of the sensor at its installation place. The greatest influence on the sensor location (point 3) was unbalanced motion of the vibrating sieve. The corresponding

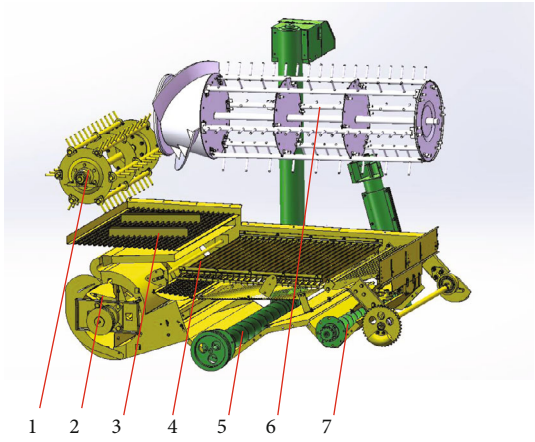

1-tangential thresher, 2-fan, 3-grain pan, 4-vibrate sieve, 5-grain auger, 6 -longitudinal thresher cylinder 7-tailing auger

Figure 1: Schematic image showing a new type of rice threshing and cleaning system.

Table 1: Location of the measurement point.

No.	Location	Working condition	Engine condition
1	Threshing rotor bearing	Soft field	Full throttle
2	Vibrating sieve drive shaft bearing	Soft field	Full throttle
3	Loss sensor location	Soft field	Full throttle

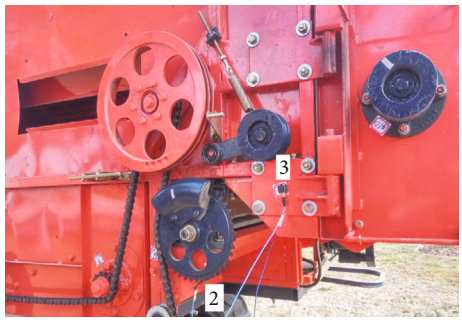

Figure 2: Location of the acceleration sensors on the combine harvester.

diagram for points 2 and 3 has shown that the excitation frequency of the vibrating sieve was 7.32 Hz and 14.65 Hz in the X direction spectrum should be the double frequency of the vibrating sieve excitation frequency.

In the X direction, although the excitation frequency at the sensor installation place was 5.86 Hz which is close to the excitation frequency of the vibrating sieve, the vibration amplitude was 0.93 m/s^2. The excitation frequency of the vibrating sieve (point 2) was 7.32 Hz with a corresponding amplitude of 1.92 m/s^2 in the Z direction, and the excitation frequency at the installation of the sensor (point 3) was 7.32 Hz. The vibration at the installation place of the Z direction sensor comes from the oscillation of the vibrating sieve with an amplitude of 2.22 m/s^2. From the above analysis, it can be known that the vibration in the sensor installation place was mainly affected by the inertia force of the vibrating sieve. If the inertia force of the vibrating sieve was strong or a suitable vibration isolation device is not adopted, the grain collision signal will be submerged in the vibration noise.

Suppressing vibration source is the most active measure to eliminate or reduce vibration. In this paper, the reciprocating motion of vibrating sieve is the source of vibration, so vibrating sieve inertial force balancing is one of the key means to suppress vibration. Complete balance and partial equilibrium are the main methods used to balance the inertial force [13]. However, complete balance is not a suitable method for oscillating sieve vibration balance that is because the counterweight may outweigh the mechanism itself and the interference caused by the counterweight can affect the normal functioning of other parts directly or indirectly. Even if the oscillating sieve could achieve complete balance, this complete balance would lead to input torque, causing the counterforce of the connecting frame pair to increase considerably. Therefore, considering the actual structure of the oscillating sieve, the partial equilibrium method is used in this paper to suppress the vibration [14, 15].

2.3. Inertia Force Balance of Vibrating Screen

2.3.1. Inertial Force and Counterweight of the Slider-Crank Mechanism. The vibrating sieve in combine harvesters can be simplified into a crank slider mechanism. Since the crank length is smaller than the connecting rod length (about 1 : 100), the slider moving direction can be considered the same direction of the crank rotation center. Therefore, crank sliding block mechanism (as shown in Figure 3) is used to analyze the vibrating sieve moving process in this paper [15].

Assuming the crank and connecting rod masses are m_1 and m_2, respectively, and m_3 is the slider mass, the corresponding mass centers are S_1 and S_2, respectively. The mechanism inertia acts on place B and place C can be expressed as

$$\begin{cases} m_{\mathrm{B}} = \dfrac{c}{l} m_1 + \dfrac{b}{l} m_2, \\ m_{\mathrm{C}} = \dfrac{a}{l} m_2 + m_3. \end{cases} \tag{1}$$

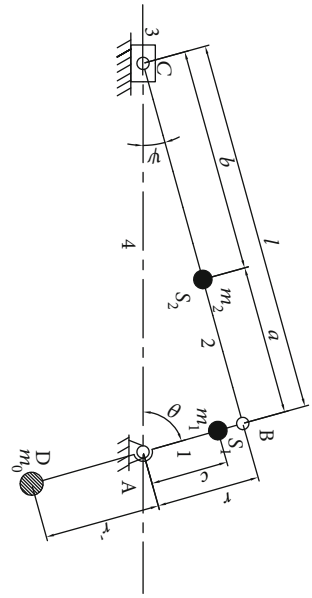

Figure 3: Schematic image showing the counterweight of an in-line slider-crank mechanism.

The slider displacement can be expressed as follows:

$$S = r\cos\theta + l\left(1 - \lambda^2 \sin^2\theta\right)^{1/2}, \tag{2}$$

where r is the crank length, θ is the crank rotation angle, λ is the ratio of connecting rod length to crank length, and $\lambda = 0.01$ in this paper.

The rotating inertial force in point B and moving inertial force in point C can be expressed as

$$\begin{aligned} F_{\mathrm{B}} &= m_{\mathrm{B}} r \dot{\theta}^2, \\ F_{\mathrm{C}} &= m_{\mathrm{C}} \rho \dot{\theta}^2 (\cos\theta + \lambda\cos 2\theta). \end{aligned} \tag{3}$$

Generally, the partial inertia force can be balanced by adding the counterweight in the sieve crank, and the rotation inertial force F_B can be balanced by the mass in point D:

$$m_{\mathrm{D1}} = \frac{r}{r'} m_{\mathrm{B}}. \tag{4}$$

Similarly, for the moving inertia force generated in the horizontal direction, an additional balance mass (m_{D2}) can be added, but the increased balance mass can balance the horizontal inertia force. However, it also produces an unnecessary vertical inertia force and cannot balance the second-order inertia force, as the second-order inertia force generated by this mechanism can be negligible. Inertial force and vertical inertial force caused by m_{D2} in a horizontal direction can be expressed as

$$\begin{cases} F_{\mathrm{x}} = m_{\mathrm{D2}} r' \dot{\theta}^2 \cos\theta, \\ F_{\mathrm{x}} = m_{\mathrm{D2}} r' \dot{\theta}^2 \sin\theta. \end{cases} \tag{5}$$

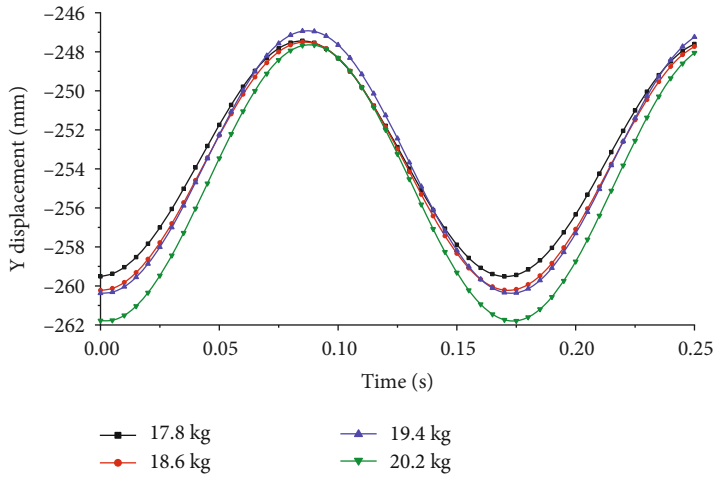

Figure 4: Displacement of the mass center in the Y direction.

Comprehensively, a coefficient $k(k = 1/3\text{-}1/2)$ was used to balance the horizontal inertial force when the corresponding vertical inertial force was relative small, by multiplying it to m_{D2}. Based on the above analysis, the counterweight is composed of two parts, that is, m_{D1} and km_{D2}:

$$m_D = m_{D1} + km_{D2} = \frac{r}{r'}(m_B + km_C). \quad (6)$$

For this sieve slider-crank mechanism model, the corresponding crank length is 16.5 mm with a mass of 5.5 kg, and the crank mass center is located at a place with a distance of 13.2 mm from point A; the revolution speed is 350 rpm in the working process. The oscillating sieve structure diagram is shown in Figure 4. The connecting rod length is 1826 mm with a mass of 102.04 kg, and the mass center is located at a place with a distance of 665 mm from point C. The rolling wheel mass is 0.26 kg. Thus, the counterweight to the sieve can be installed in the reversed direction of the crank with $r' = 95$ mm. At last, the counterweight is distributed in the range of 17.8 kg-20.2 kg.

2.3.2. Simulation of Optimum Counterweight for Inertial Force Balance. To overcome limitations and inaccuracies caused by calculation, the dynamic software ADAMS (MSC, Newport Beach, USA) was used to analyze the motion law of the mass center and the effect of reciprocating motion on the frame force in the process of the shaker moving, and the optimum counterweight mass of the shaker can be obtained. The fundamental goal of inertial force balance was to make the total center of mass as small as possible or tends to a point (that is, the center of mass static). According to this idea, the total center of this part tends to be stable by adding different balancing massed in the simulation process. To make sure the simulation result can be closer to the actual mechanism motion, the assembled sieve model was imported into the ADAMS software [16], shown in Figure 5.

The motion pair between the vibrating board and eccentric shaking shaft was set as a rotating pair, the motion pair between the counterweight and sprocket wheel was a fixed pair, the motion pair between the roller and guide rails fixed on the frame was a moving pair, and the motion pair between the vibrating board and the roller was a rotating pair. To reflect the influence of the inertial force on the frame, a side board was set as the frame and fixed on the ground, and the motion pair between the side board and the eccentric shaking shaft was a rotating pair. During the simulation process, the eccentric shaking shaft speed was 2100 degrees/s (350 rpm). The simulation time was 1.0 s, and the step size was 0.01 s. During the simulation process, the revolution speed of the eccentric shaking shaft is 2100 degrees/s (350 rpm).

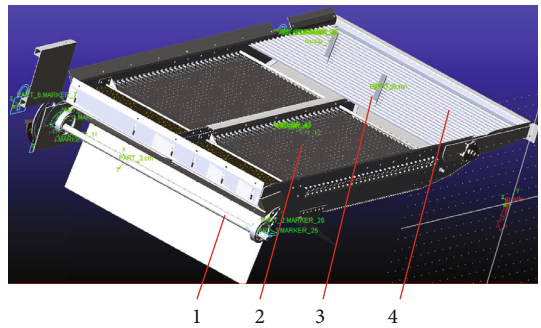

1-driving shaft, 2-sieve, 3-guide plate, 4-grain pan

Figure 5: Simulation model of the oscillating sieve.

Taking 17.8 kg, 18.6 kg, 19.4 kg, and 20.2 kg as counterweight measurements, the coordinate variation of the mass center is shown in Figures 4 and 6. As there was no displacement in the Z direction, the movement tracks of the mass center were determined in the X and Y dimensions shown in Figures 7 and 8.

From Figures 6–8, it can be seen that the horizontal displacement decreases from 32 mm to 8 mm, the vertical displacement decreases from 17 mm to 13 mm after adding the counterweight, and the total sieve mass center trajectory range decreases obviously. On the other hand, the trajectory of the mass center is different under different balanced counterweights. When the counterweight mass is 18.6 kg, the

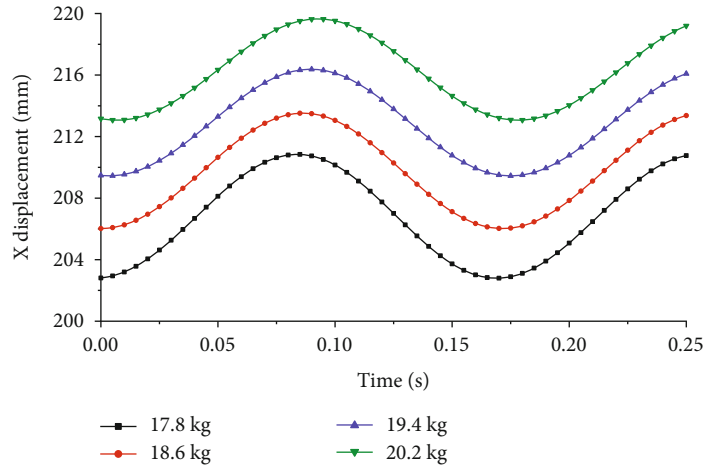

Figure 6: Displacement of the mass center in the X direction.

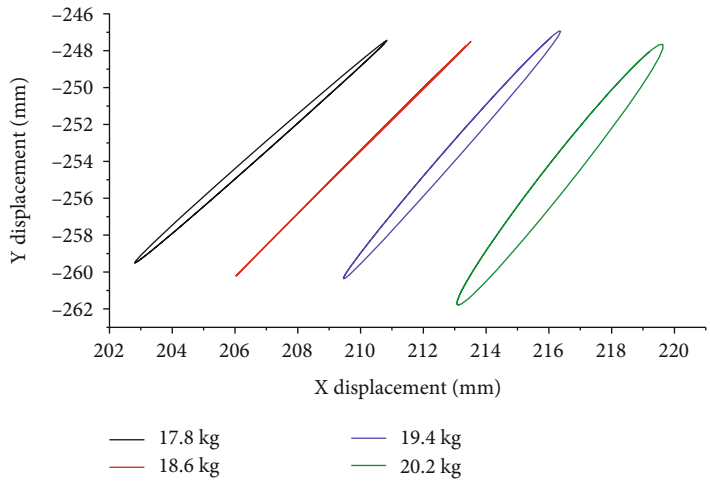

Figure 7: Tracks of the mass center under different counterweights.

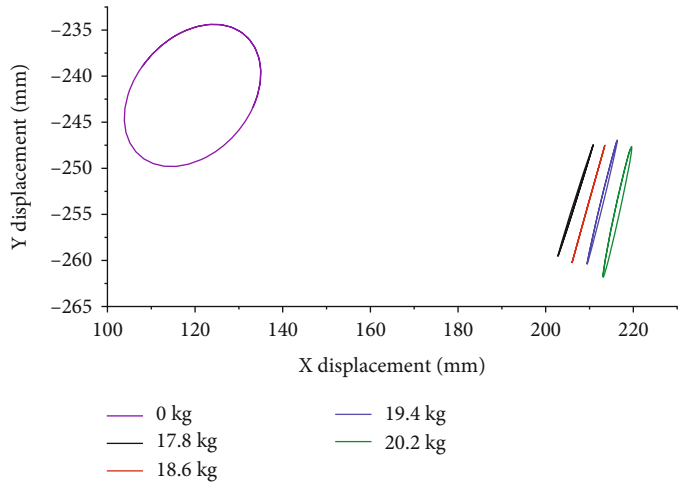

Figure 8: Total mass center trajectory of vibrating screen without counterweight and with counterweight.

range of motion of the center of mass is the smallest, and the corresponding balancing effect is the best. Therefore, it can be considered that the best counterweight of the sieve is 18.6 kg.

To indicate the inertial force value during vibration accurately, the counterforce in the X and Y directions at joints and the inertial force was obtained under different

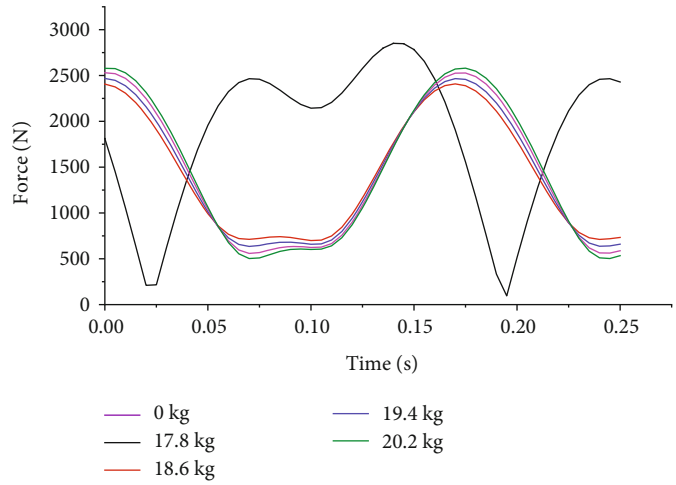

Figure 9: Total force of vibrating screen without counterweight and with counterweight.

counterweights, shown as Figure 9. The relationship between counterweights and the total force under different counterweights are shown Table 2.

From Table 2, it can be known that the total force, in terms of mean, RMS, or peak value, has a great reduction after adding counterweight, indicating partial inertial force was balanced. When the balanced mass was 17.8-18.6 kg, the corresponding RMS and peak value of the total force are relatively small, as the motion range of the mass center was the smallest when the counterweight mass was 18.6 kg. Therefore, 18.6 kg can be considered as the best balance mass to vibrating sieve.

3. Passive Vibration Isolation

3.1. Governing Equation. From Section 2, it can be known that the main vibration frequency was 7.32 Hz in the Z direction with an amplitude of 2.22 m/s^2, the second-order vibration frequency was 12.21 Hz in the Z direction with an amplitude of 1.30 m/s^2, and the third-order vibration frequency was 26.4 Hz in the Z direction with an amplitude of 0.28 m/s^2 after vibration suppressed by adding mass to the sieve. However, the vibration amplitude is still much higher in the first- and the second-order mode shapes. Therefore, it is necessary to take some actions to suppress the vibration in the Z direction.

Vibration isolation is to set up a vibration isolation system or device between the vibration source and the vibration body to reduce or isolate the vibration transmission. There are two kinds of vibration isolation method: one is vibration isolation from mechanical support to foundation, which is called active vibration isolation. The other is to weaken or prevent the vibration of the foundation to be transmitted to the static equipment to be protected, so as to reduce the transmission of motion, called passive vibration isolation. This paper mainly studied the passive vibration isolation, that is, to reduce the vibration transmitted by the frame to the sensor through the connecting structure. Supposing the exciting force acted on the support plate of

Table 2: Total force under different counterweights.

Mass (kg)	Min. (N)	Max. (N)	Average (N)	RMS (N)	Peak (N)
0	249	2850	1887	2251	2601
17.8	699	2406	1452.6	51	753.6
18.6	635	2467	1462	65	1832
19.4	561	2530	1474.44	59	913.44
20.2	503	2578	1486	57	983

the sensor is $y(t) = |Y| \sin \omega t$ in a passive vibration isolation device, the dynamic equation of the isolation model can be expressed as:

$$m\ddot{x}(t) + c\left[\dot{x}(t) - \dot{y}\right] + k[x(t) - y] = 0. \tag{7}$$

The displacement can be expressed as

$$x(t) = \frac{k + i\omega c}{k - m\omega^2 + i\omega c}|Y|e^{i\omega t} = |H_A(\omega)|e^{-i\varphi A}y(t), \tag{8}$$

where

$$T_A = |H_A(\omega)| = \sqrt{\frac{1 + [2\xi(\omega/\omega_n)]^2}{\left[1 - \left((\omega/\omega_n)^2\right)\right]^2 + [2\xi(\omega/\omega_n)]^2}}, \tag{9}$$

$$\varphi_A = \arctan \frac{2\xi(\omega/\omega_n)^3}{1 - (\omega/\omega_n)^2 + [2\xi(\omega/\omega_n)]^2}, \tag{10}$$

$$k = \omega_n^2 m. \tag{11}$$

T_A is called the vibration isolation transmission efficiency, and with the smaller T_A, the vibration suppression system can get a more ideal vibration isolation effect. From Equation (11), it can be learnt that the vibration isolation device can get a good effect as $(\omega/\omega_n) > \sqrt{2}$, the corresponding $T_A < 1$. The larger the ω/ω_n, the better the vibration

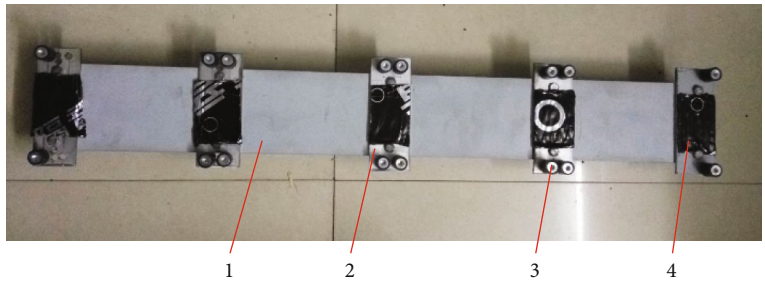

1-support plate, 2-transverse connecting plate,
3-longitudinal vibration isolation rubber, 4-damping material.

Figure 10: Monitoring board supporting structure.

isolation effect. Generally speaking, the ideal $\omega/\omega_n = 2.5\sim5$ in an engineering area [17].

3.2. Design of the Vibration Isolation Device. It is found that the calculated value will be very small if there is no support or the support mass is small. In practice, it cannot play a supporting role at all. To solve the above problems, the mass vibration isolation method was adopted to reduce the vibration transmission by increasing the mass of the support plate and the transverse connecting plate, so as to increase the integral stiffness of the isolation rubber. The calculated rubber stiffness was between 5000 and 15000 N/m, and the system frequency was 3-10 Hz after adding the support mass. The VD type vibration isolation rubber from Suzhou Xuan Xin Rubber and Plastic Products Co., Ltd. was selected as the vibration isolation material; the size is 15 mm × 15 mm × 15 mm. Although the vibration amplitude in the X direction is small, considering that other vibration disturbances may be received during the working process, the vibration isolation rubber is selected according to the above vibration isolation principle and formula, and the VV type vibration isolation rubber with a size of 20 mm × 25 mm × 20 mm is selected. The monitoring board supporting structure is shown in Figure 10.

Figure 11 is a signal collected by UNI-TUPO2 000CS series digital storage oscilloscopes after vibration isolation during grain collision. Using the voltage amplitude of the output signal is easier to compare the effect. Moreover, the amplitude of the signal also is an important factor to determine the threshold of the signal processing circuit. From Figure 11, it can be learnt that the disturbance signal amplitude after vibration isolation is about 50 mV, while the grain collision signal voltage amplitude was above 3 V, the influence of the vibration can be overcome if we set the threshold of comparative voltage of the signal processing circuit at 1 V. It can be seen that vibration isolation plays an active role in reducing vibration disturbance and highlighting grain signal.

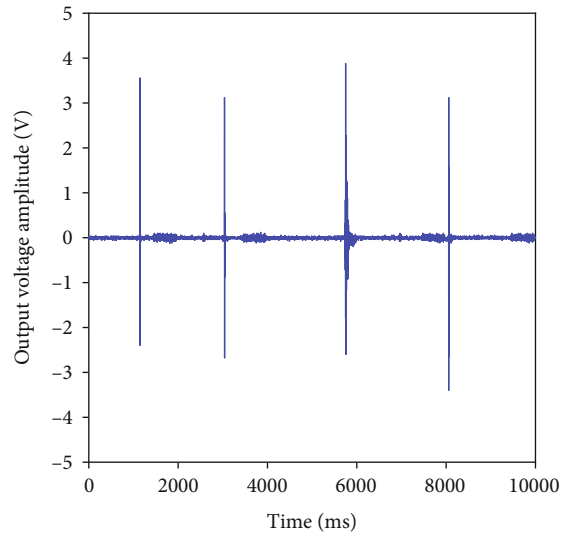

Figure 11: Signal characteristic after vibration isolation.

4. Conclusion

(1) Inertia force from sieve unbalanced motion has the greatest effect on the monitoring accuracy of the sensor. The exciting frequency of the vibrating screen is 7.32 Hz, and 14.65 Hz in the X direction spectrum should be the frequency doubling of the vibrating screen's exciting frequency; in the X direction, although the exciting frequency at the sensor installation is 5.86 Hz close to the vibrating sieve's exciting frequency, the influence is not so severe

(2) The best balance mass is 18.6 kg for the vibration sieve; the corresponding mean, RMS, and peak-peak values are relatively small; and the corresponding mass center trajectory range was the smallest

(3) The ideal vibration isolation rubber stiffness is in the range of 5000 N/m-15000 N/m, and the system corresponding natural frequency is 3-10 Hz. Experiments showed that the disturbance signal amplitude after vibration isolation is about 50 mV, which verified that vibration isolation plays an active role in reducing vibration disturbance and highlighting grain collision signal

Nomenclature

a_C: Acceleration in point C ($m \cdot s^{-2}$)
θ: Crank rotation angle (°)
ω_n: Inherent rotational velocity ($rad \cdot s^{-1}$)

F_B: Rotating inertial force in point B (N)
F_C: Moving inertial force in point C (N)
F_{D1}: Balanced by the mass in point D (N)
λ: Rod and crank length ratio
k: Coefficient ($N \cdot m^{-1}$)
r: Crank length (mm)
r': Length of added mass to crank mass center (m)
$x(t)$: Displacement of the sensor (mm)
ξ: Damping coefficient
c: Damping of the vibration isolator
F_x: Inertial force caused by m_{D2} (N)
F_y: Vertical inertia force caused by m_{D2} (N)
m_{B1}: Mechanism inertia acts on place B from m_1 (kg)
m_{B2}: Mechanism inertia acts on place B from m_2 (kg)
m_1: Crank mass (kg)
m_2: Connecting rod mass (kg)
m_3: Slider mass (kg)
$y(t)$: Exciting force on the support plate (N)
k: Stiffness of the vibration isolator ($k \cdot N^{-1}$)
ω: Rotational velocity of the vibration ($rad \cdot s^{-1}$)
S: Slider displacement (m)
S_1: Rod-crank 1 mass center (m)
S_2: Rod-crank 2 mass center (m)
m_{D1}: Additional balance mass 1 (kg)
m_{D2}: Additional balance mass 2 (kg)
T_A: Vibration isolation transmission efficiency
φ_A: Frequency characteristic ($rad \cdot s^{-1}$).

Data Availability

As the data from the ADAMS simulation can only be derived from the corresponding software and the vibration test data file can only be opened by a licensed software, the data used to support the findings of this study are available from the corresponding author upon request (the corresponding author's email is liangzhenwei518@126.com).

Conflicts of Interest

We confirmed that the mentioned received funding did not lead to any conflict of interests regarding the publication of this manuscript. Also, there is no any other possible conflict of interests in the manuscript.

Acknowledgments

This research was supported by the National Key Research and Development Program of China (2016YFD0702101), the Jiangsu Agriculture Science and Technology Innovation Fund (JASTIF) (CX(19)3083), a project funded by the Synergistic Innovation Center of Jiangsu Modern Agricultural Equipment and Technology, China (4091600027), a project funded by the China Postdoctoral Science Foundation (2019 M651746), and a project funded by the Priority Academic Program Development of Jiangsu Higher Education Institutions (No. PAPD-2018-87).

References

[1] G. Bernhardt, "Apparatus and method for determining loss in combine harvester," 2005, US Patent 6869355.

[2] G. Craessaerts, J. de Baerdemaeker, B. Missotten, and W. Saeys, "Fuzzy control of the cleaning process on a combine harvester," *Biosystems Engineering*, vol. 106, no. 2, pp. 103–111, 2010.

[3] G. Craessaerts, W. Saeys, B. Missotten, and J. de Baerdemaeker, "Identification of the cleaning process on combine harvesters, part II: a fuzzy model for prediction of the sieve losses," *Biosystems Engineering*, vol. 106, no. 2, pp. 97–102, 2010.

[4] K. W. Eldredge, "Grain Loss Indicator," 1985, U.S Patent 4490964.

[5] N. L. D. Ing, O. D. D. Ing, and P. E. D. Ing, "Combine harvester grain loss monitor - electronics with loss mass per unit area indicator and grain mass adjuster," 1976, D E Patent 2527090.

[6] C. Liu and J. Leonard, "Monitoring actual grain loss from an axial flow combine in real time," *Computers and Electronics in Agriculture*, vol. 9, no. 3, pp. 231–242, 1993.

[7] K. Maertens, H. Ramon, and J. De Baerdemaeker, "An on-the-go monitoring algorithm for separation processes in combine harvesters," *Computers and Electronics in Agriculture*, vol. 43, no. 3, pp. 197–207, 2004.

[8] G. Strubbe, "Grain loss sensor for combine harvester," 1991, U.S Patent 5046362.

[9] X. Zhou, R. Zhu, X. Zhou, and Y. Tang, "The nonitoring system for cleaning loss of the grain combine harvester based on sensor technology," *Journal of Agricultural Mechanization Research*, vol. 2, pp. 1–3, 2010.

[10] H. T. Zhang and X. H. Li, "Research on the balance effect of shaker used in combine harvester," *Mechanical Research & Application*, vol. 1, pp. 63-64, 2010.

[11] L. Xu, C. Wei, Z. Liang, X. Chai, Y. Li, and Q. Liu, "Development of rapeseed cleaning loss monitoring system and experiments in a combine harvester," *Biosystems Engineering*, vol. 178, pp. 118–130, 2019.

[12] Z. Tang, H. Zhang, and Y. Zhou, "Unbalanced vibration identification of tangential threshing cylinder induced by rice threshing process," *Shock and Vibration*, vol. 2018, Article ID 4708730, 14 pages, 2018.

[13] V. Arakelian and S. Briot, "Simultaneous inertia force/moment balancing and torque compensation of slider-crank mechanisms," *Mechanics Research Communications*, vol. 37, no. 2, pp. 265–269, 2010.

[14] C. Kailash and C. Himanshu, *Optimum balancing of slider-crank mechanism using equimomental system of point-masses Department of Mechanical Engineering*, Malaviya National Institute of Technology Jaipur, Jaipur, India, 2017.

[15] C. Wei, L. Xu, J. Wang, and Y. Li, "Inertial force balance and ADAMS simulation of the oscillating sieve and return pan of a rice combine harvester," *International Journal of Agricultural and Biological Engineering*, vol. 11, no. 1, pp. 129–137, 2018.

[16] W. D. Guo, *Virtual Prototyping Technology and ADAMS Application Examples Tutorial*, BeiHang University Press, Beijing, 2008.

[17] Z. W. Liang, *Study on grain separation loss monitoring sensor for axial flow combine harvester, [M.S thesis]*, Jiangsu University, Zhenjiang, China, 2010.